Effect of Methane Mitigation on Global Temperature under a Permafrost Feedback

Hannah Bäck[1,a*], Riley May[2,a*],
Divya Sree Naidu[3], and Steffen Eikenberry[3]

[1] *University of Iowa*
[2] *Utah State University*
[3] *Arizona State University*
[a] *Simon A. Levin Mathematical, Computational, and Modeling Sciences Center: Quantitative Research for the Life & Social Sciences Program, Arizona State University*
[*] *Equally contributing authors*

July 21, 2022

Abstract

Recent works in climate science emphasize the importance of stewardship to maintain Earth in a safe operating space for supporting human life. Earth systems may fall into a undesirable system state if certain boundaries are crossed. If 1.5°C warming is exceeded, it may cause a cascade of effects, such as permafrost melt, Amazon forest dieback, and ice sheet collapse. The permafrost is a tipping element that is particularly vulnerable to warming in the near term and has substantial feedback into climate. Methane (CH_4) is a short-lived greenhouse gas but has the global warming potential of 28.5 times that of carbon dioxide (CO_2) over a 100 year time span. Because permafrost thaw in the coming centuries is partly determined by the warming of the 21st century, rapid reductions in methane emissions early in the 21st century could have far reaching effects. We use a reduced complexity carbon cycle model and a permafrost feedback module to explore the possibility that accelerating reductions in methane emissions could help us avoid long-term warming by limiting permafrost melt. We simulate 3 extended RCP emission scenarios (RCP 2.6, 4.5, and 6) through the year 2300 and impose methane mitigation strategies where we reduce CH_4 emissions by 1%, 5% or 10% annually until the long-term scenario emission level is reached. We find that accelerated rates of methane mitigation will not sufficiently bend the global temperature anomaly to prevent or delay a permafrost feedback, nor do they result in a meaningful long term reduction in temperatures. We find that the magnitude of methane mitigation (i.e., long-term emission level) and not the rate of reduction, corresponds to long term temperature change. Therefore, policy and mitigation efforts should emphasize durable decreases in methane emissions over rapidity of implementation.

1 Introduction

1.1 Earth's Safe Operating Space

Paleoclimate data suggest that the current Holocene epoch is uniquely conducive to supporting human life. The current inter-glacial era beginning 11,700 years ago has been uniquely warm and stable; therefore, well equipped to support our agricultural system [26]. Now, human actions in the form of greenhouse gas emissions, land use, fertilizer use, novel entity pollution etc. have altered the trajectory of our Earth system and may be pushing out of this previously stable operating space. Humans decisively took the wheel in 1950 where there was a "great acceleration" of economic intensity, and, correspondingly, an increase of environmental externalities [23]. Humans are increasingly driving natural geophysical processes in this new Anthropocene era.

Given that humans are now a driving force for Earth systems, we must understand what climate tipping points we need to urgently avoid, and the ways in which we can avoid them. There are tipping elements that react to warming quickly (fast-onset tipping elements), such as Amazon rain forest dieback, and slow-onset tipping elements, such as the Atlantic Meridional Overturning Circulation (AMOC). These, while they may have the same temperature threshold, may not "tip" for centuries to come [19]. Because tipping elements may have some level of inertia, it may be possible to temporarily overshoot a tipping point while still maintaining system stability provided the duration of time in the overshoot is small and temperatures ultimately stabilize at a safe level [19].

1.2 Planetary Boundaries

While determining the climate boundary, we must consider positive feedbacks, such as ice sheet loss, permafrost melt, Atlantic ocean circulation, and Amazon rainforest dieback [13]. Without these feedbacks, previous estimates lay between 2-3°C for "safe warming." With the inclusion of positive, interacting feedbacks, Lenton et al. (2019) states that warming must be limited to 1.5°C [13]. Warming past 1.5°C may cause runaway feedback effects.

In this paper, we focus on the effect of anthropogenic emissions on the climate boundary, but there are other important interlinked planetary boundaries (biosphere integrity, land system change, ocean acidification, etc.) [22]. The biosphere integrity and climate change boundaries are at high risk, and there is increasing danger in exceeding their thresholds. Each Earth system has a boundary that may be quantified differently; while the climate boundary may be measured in terms of simple degrees of warming, biosphere integrity is more complicated to quantify.

It is important to note that some boundaries, such as land system change or ocean acidification, have direct effects on climate. As the ocean acidifies due to increased CO_2 emissions and additional carbon uptake, its ability to absorb additional carbon will weaken, which is reflected in our model (see section 2.4). As our land use increases, the decreased extent of biota and increase in exposed soil will result in a smaller terrestrial carbon sink. Crossing any boundary decreases Earth system resiliency as a whole and pushes us further out of our stable equilibrium. When viewed as simple "ball and cup" resiliency, each boundary crossed nudges us further towards a new system state.

1.3 Climate Feedbacks

We also must consider what feedback is most important in the short term. Currently, global average temperatures are roughly 0.8-1.3°C above pre-industrial according to the IPCC [3]. Long-term warming is a function of cumulative carbon emissions, therefore, the concept of the carbon budget was developed to balance our projected carbon emissions versus degrees of warming. The carbon budget describes a total cumulative amount of carbon that can be emitted to limit warming to 1.5°C. Each year, anthropogenic CO_2 emissions take roughly 9 GtC off the budget. In 2019, there was an estimated 500 GtC left in the "budget", [13] [20], but more recent estimates from 2021 posit only 420 GtC remaining [7].

The permafrost may be the most important feedback to look at in the short term because of its high net carbon content and its sensitivity to degradation with increased warming. As temperatures rise, permafrost emissions could push us over the carbon budget. While there is some uncertainty, it is estimated that the intact permafrost stored a total of 1035 gigatonnes of carbon (GtC) [12]. The IPCC has created emission scenarios, representative concentration pathways (RCPs) corresponding

to the change in radiative forcing the Earth will experience at the year 2100 (i.e, under RCP 8.5, the Earth will experience +8.5 watts/m^{-2} of radiative forcing). One study indicates that under an RCP 8.5, 33-114 GtC may be released by 2100, contributing to an additional warming of 0.04-0.23°C [21], and by 2300, half the vulnerable permafrost carbon stock could be released. While the RCP 8.5 is a high end scenario, there is still a great deal of uncertainty regarding permafrost carbon stocks, thawing processes, and subsequent microbial decomposition of CO_2 and CH_4 , as well as other potential feedbacks. Another study found with high uncertainty that 100 GtC could be released from the permafrost by 2100, accounting for roughly 24% of our remaining carbon budget [7]. For this reason, permafrost feedback is the primary positive climate feedback we examine in this paper.

1.4 Mitigation Priorities

Because near term climate forcers like methane have relatively short atmospheric lifetimes, mitigating annual emissions of these substances is more relevant than a net cumulative budget. We are concerned with net cumulative emissions of CO_2 because it is a millennial gas that does not breakdown in the atmosphere, where in contrast, methane oxidizes in the presence of hydroxyl radicals (OH) and has a perturbation lifetime of approximately 12 years [25]. Therefore, we are more concerned with atmospheric concentrations of methane at any given time, and thus, limiting annual emissions rather than a net cumulative amount.

Given that warming is a function of all anthropogenic emissions, mitigating methane will play a role in avoiding the climate boundary. Methane is a powerful greenhouse gas and is responsible for about 1.19 W/m^{-2} of radiative forcing since 1750. According to Pierrehumbert et al. (2014), methane mitigation is not a substitute for an immediate decarbonization plan. Yet, there are still questions regarding methane mitigation and its role *in addition to decarbonization*: Is there a target level of annual CH_4 emissions that should be reached? Does it matter how fast we can reduce emissions to lower levels?

We seek to answer the question of rate of methane mitigation: Is there any benefit to an accelerated emissions reduction plan? We are interested in the possibility that the mitigation of methane could prevent some release of CO_2 from the permafrost and therefore mitigate long-term warming. Because methane has considerable short term temperature effects, it could slow the rate of warming and warrants examination in relation to the permafrost feedback.

We use a reduced complexity model that represents the most relevant Earth systems to understand the dynamics between reducing annual CH_4 emissions and long term temperature changes from CO_2 , CH_4 , and nitrous oxide (N_2O), due to its interaction with methane. Radiative forcing attributable to our three greenhouse gases is described with IPCC formulas and a two box ocean layer heat transfer model. We develop a simplified carbon cycle model based on Glotter et al. (2014) and Hartin et al. (2015, 2016) that describes flux between three terrestrial biota compartments and two ocean compartments. Increased carbon uptake due to CO_2 fertilization and CO_2 buffering with acidification are included. We model permafrost decomposition as a linear decrease in extent with rise in temperature and subsequent release of emissions as exponential decay based on the model of Kessler et al. (2017), where permafrost carbon mobilization to a labile carbon pool increases linearly with temperature. Carbon in this labile pool is then emitted to the atmosphere as a mix of CO_2 and CH_4 according to exponential dynamics with an e-folding time of about 70 years.

These simplified representations of Earth systems describe the relationship of emissions to temperature perturbation. We then drive the model using RCP CO_2 emission time-series while varying rates of methane mitigation to determine the impact on long term temperature. We find that the magnitude of methane mitigation (i.e., the final long-term sustained methane emission rate that is able to be attained) has a relationship to long term temperature, and not the rate of mitigation (i.e, how quickly this final rate is able to be attained).

2 Methods

We use a reduced climate complexity model implemented with coupled first order differential equations. These equations model the carbon cycle with carbon fluxes between atmospheric, terrestrial, and ocean layers, along with ocean carbonate chemistry. We use a simple two box temperature response model to calculate the effects of radiative forcing from CO_2 , N_2O , and CH_4 on surface temperature. We include a two part linear permafrost feedback using a differential equation that responds to increases of the global mean temperature. In the model, temperature responds to either imposed concentrations when driving the model with historical data or emissions when projecting the model.

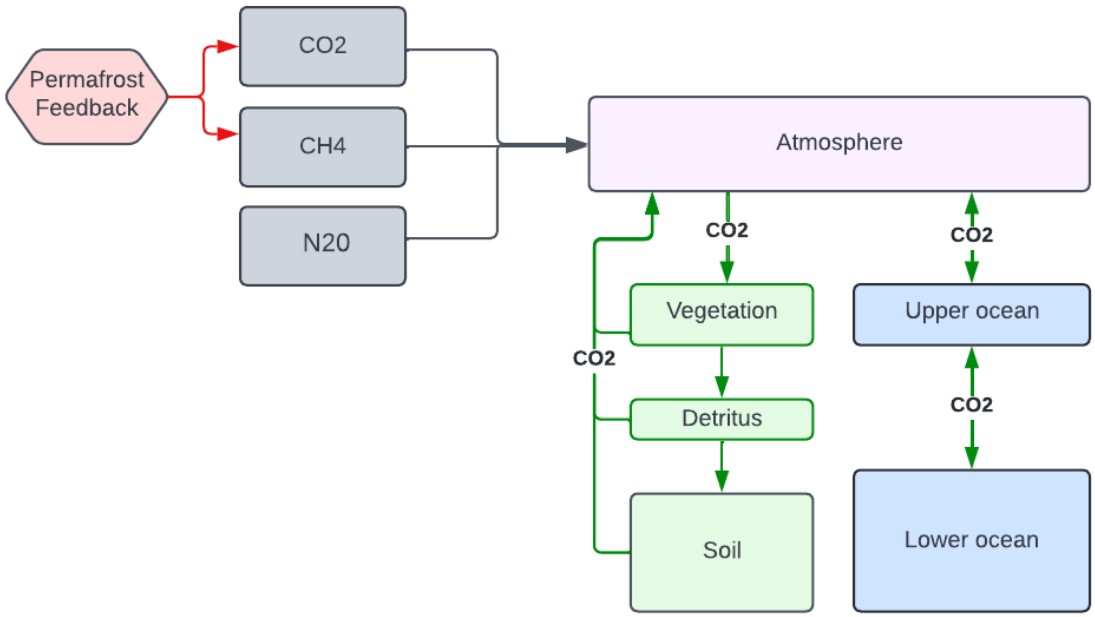

Figure 1: Model outline: We look at CO_2 , CH_4 , and N_2O emissions into the atmosphere. Note, methane emissions come from anthropogenic and biogenic (natural) sources, and from permafrost emissions. CO_2 is from anthropogenic sources and the permafrost. N_2O is purely an anthropogenic emission. Carbon moves between the atmosphere (as CO_2), terrestrial boxes (the vegetation, detritus, and soil), and the ocean boxes (upper and lower). The upper ocean temperature is used as a proxy for surface temperature perturbation, and its temperature interacts with the heat sink of the lower ocean. Increases in temperature amplify permafrost emissions.

Figure 1 shows a simplified representation of our model's dynamics. Anthropogenic emissions, from fossil fuels and land use change, and the permafrost feedback are the primary sources of CO_2 and CH_4 emissions, our primary warming agents. Biogenic methane emissions are included as a baseline, non-mitigable CH_4 source that contributes to warming, set at a constant 300 Mt CH_4 per year, between the 220-368 Mt estimated by Jackson et al. (2020) [11]. CO_2 circulates between the terrestrial and ocean compartments. Temperature perturbation is calculated from the change of radiative forcing from emissions which warm the upper and, in turn, the lower ocean. This temperature increase then feeds back into the permafrost module, causing permafrost melt and subsequent release of methane and CO_2 .

2.1 The Carbon Cycle

Terrestrial Carbon Stores

The terrestrial carbon stores included in our model are the vegetation, detritus and soil. Together, these have a significant interaction with atmospheric carbon. We use a differential equation to describe

each major box, where C_V is the carbon of the vegetation layer, C_D is the carbon in the detritus layer, and C_S is the carbon in the soil layer. Each box (Equations (1), (2), (3)) has a source term representing net primary productivity (NPP), where the autotrophs store some of amount of carbon. Each layer also has loss and source terms to describe transfer of carbon from one layer to another. The vegetation box has a loss term representing the flux of carbon to the detritus ($C_V f_{vd}$) and soil ($C_V f_{vs}$) layers. The detritus box has a loss term for the carbon flux to the soil layer ($C_D f_{ds}$). The soil and detritus boxes have loss terms for heterotrophic respiration (RH), where microbial activity release carbon into the atmosphere. Finally, each layer has a term representing losses of carbon due to land use change (F_{LC}).

We use formulas from Hartin 2015[10] given by

$$\frac{dC_V}{dt} = \text{NPP} f_{nv} - C_V(f_{vd} + f_{vs}) - F_{LC} f_{lv} \ , \tag{1}$$

$$\frac{dC_D}{dt} = \text{NPP} f_{nd} + C_V f_{vd} - C_D f_{ds} - \text{RH}_{det} - F_{LC} f_{ld} \ , \tag{2}$$

$$\frac{dC_S}{dt} = \text{NPP} f_{ns} + C_V f_{vs} + C_D f_{ds} - \text{RH}_{soil} - F_{LC} f_{ls} \ . \tag{3}$$

Any land use change alters the CO_2 content of the terrestrial stores. For example, if land is deforested, each layer will release some carbon into the atmosphere. If x GtC are released due to land use change, a certain proportion of those emissions comes from each of the different layer represented by the portions $f_{lv}, f_{ld}, \text{and} f_{ls}$ (Table 1).

Heterotrophic respiration from the detritus and soil layers feeds into the atmosphere. RH is a function of the current carbon content of the respective strata and the respiration factor Q_{10} which is the factor by which respiration increases for a 10 degree increase in temperature. For soil and detritus, we use a ten year average of global mean temperature perturbation divided by ten. A running average is used to represent the slow change in temperature from the surface of the Earth to the lower layers of soil.

Net primary productivity (NPP) is a function of current atmospheric carbon levels compared to pre-industrial carbon levels in ppm scaled by carbon fertilization parameter β. The value for beta β varies depending on the region [9], but we use a single value to represent the whole earth system. The total NPP is subtracted from our atmospheric carbon, reflecting the carbon uptake by all terrestrial sinks. This net primary productivity is added to each of the terrestrial stores by a factor f_{nv}, f_{nd}, f_{ns} (table 1). Therefore, we determine NPP and RH by

$$\text{NPP}(t) = \text{NPP}_0 \times f(C_{atm}, \beta) \tag{4}$$

$$f(C_{atm}, \beta) = 1 + \beta \times log\left(\frac{C_{atm}}{C_0}\right) \tag{5}$$

$$\text{RH}_{s,d}(t) = C_{s,d} \times f_{rs,rd} \times Q_{10}^{T(t)/10}. \tag{6}$$

Terrestrial Carbon Stores

Parameter	Value	Description
f_{ds}	0.60	fraction of detritus that transfers to the soil
f_{ld}	0.01	fraction land use carbon that enters detritus
f_{ls}	0.89	fraction land use carbon that enters soil
f_{lv}	0.10	fraction land use carbon that enters vegetation
f_{nd}	0.60	fraction of NPP carbon that enters the detritus
f_{ns}	0.05	fraction of NPP carbon that enters the soil
f_{nv}	0.35	fraction of NPP carbon that enters the vegetation
f_{rd}	0.25	fraction of respiration carbon that enters the detritus
f_{rs}	0.02	fraction of respiration carbon that enters the soil
f_{vd}	0.034	fraction of vegetation carbon that enters the detritus
f_{vs}	0.001	fraction of vegetation carbon that enters the soil
β	0.36	carbon fertilization parameter
Q_{10}	2.45	Q_{10} respiration factor

Table 1: These parameters represent the various terrestrial stores from Hartin et al (2016). A source of adjustment for future editions of the model may include tuning the parameter β to a higher value; values for β close to 0.5 create a slightly higher carbon intake.

2.2 Oceanic Carbon Stores

Ocean buffering chemistry is modeled by the Bolin Erikson Adjusted Model (BEAM), which reflects the relationship between CO_2 in the atmosphere, upper ocean, and lower ocean which we adopt. This model takes into account the CO_2 transfer between the atmosphere and the largest carbon sink, the ocean, via general ocean turbulence.

We represent the carbon in the atmosphere, upper ocean, and lower ocean boxes as C_A, C_U, and C_L respectively. Important parameters include δ_d and δ_a, where δ_d represents the ratio of the moles in the lower (deep) to the moles of the upper ocean. Then, δ_a is the ratio of moles between the atmosphere and and the upper ocean. Given that we know that the ocean is about 500 times the size of the ocean, we set δ_d to 50 and solve for δ_a using known values for atmospheric and ocean moles. We use k_a for the turnover time for the upper ocean and k_d for the turnover time for the deep ocean. Lastly, k_H is Henry's constant. Then, there is an anthropogenic emissions stream $E(t)$ that is added directly to C_A.

To model the carbon chemistry of the ocean, we look at the dynamics of how atmospheric carbon is absorbed into the different ocean layers. The loss of carbon in the atmosphere to the upper ocean is represented by $-k_a C_A$. It re-enters the atmosphere with expression $k_a \frac{k_H}{\delta_a} C_U$. The change in the upper ocean is the same expressions with opposite signs. Additionally, there is an exchange between the upper and lower ocean given by $-k_d C_U + \frac{k_d}{\delta_d} C_L$. These flows can be represented by the equations [8]

$$\frac{dC_A}{dt} = -k_a C_A + k_a \frac{k_H}{\delta_a} C_U + E(t) \ , \tag{7}$$

$$\frac{dC_U}{dt} = k_a C_A - k_a \frac{k_H}{\delta_a} C_U - k_d C_U + \frac{k_d}{\delta_d} C_L \ , \tag{8}$$

$$\frac{dC_L}{dt} = k_d C_U - \frac{k_d}{\delta_d} C_L \ . \tag{9}$$

However, this does not completely model the dynamics between the ocean and the atmosphere. We must take into account the dynamic ocean chemistry as atmospheric CO_2 is dissolved in saltwater into the forms of bicarbonate (HCO_3^-) and carbonate (CO_3^{2-}). The dissociation of carbon into its compounds occur with dissociation constant k_1 and k_2 (see Table 2). This dynamic equilibrium is represented by [8]

$$CO_2 + H_2O \overset{k_1}{\rightleftharpoons} HCO_3^- + H^+ \overset{k_2}{\rightleftharpoons} CO_3^{2-} + 2H^+, \text{ where} \tag{10}$$

$$k_1 = \frac{[HCO_3^-][H^+]}{[CO_2(aq)]} \text{ and } k_2 = \frac{[CO_3^{2-}][H^+]}{[HCO_3^-]} \ . \tag{11}$$

Because CO_2 is a weak acid that reduces the ocean's capacity to absorb more carbon dioxide, we must determine what the ocean's carbon storage capacity is at a given time. We use Λ as this "carbon storage factor", representing the ratio of the equilibrium of total dissolved inorganic carbon to CO_2 (aq). Because we have the dissociation constants k_1 and k_2, Λ also can be described as a function of hydrogen ion concentrations at a given time, and we get the following [8]:

$$\Lambda(t) = \frac{[CO_2] + [HCO_3^-] + [CO_3^{2-}]}{[CO_2]} = 1 + \frac{k_1}{[H^+]} + \frac{k_1 k_2}{[H^+]^2}. \tag{12}$$

Also, Λ is the ratio of the equilibrium of sum of dissolved inorganic carbon (DIC) relative to CO_2 (aq).

To find Λ, we must know the concentration of hydrogen ions. By definition, we have the total dissolved inorganic carbon as

$$[DIC] = [\mathrm{CO}_2(aq)] + [HCO_3^-] + [CO_3^{2-}] \ . \tag{13}$$

After some simple algebraic manipulation of the equations for k_1 and k_2 on (11) and plugging into our $[DIC]$ on (13), we get

$$[DIC] = [\mathrm{CO}_2(aq)] \left(1 + \frac{k_1}{[H^+]} + \frac{k_1 k_2}{[H^+]^2}\right) \ . \tag{14}$$

Because the charges of the ions must be balanced, we can calculate the our $[H^+]$ concentration using the alkalinity (Alk) as

$$Alk = [HCO_3^-] + 2[CO_3^-] = [\mathrm{CO}_2(aq)] \left(\frac{k_1}{[H^+]} + \frac{2k_1 k_2}{[H^+]^2}\right) \tag{15}$$

$$= \frac{C_U}{\Lambda} \left(\frac{k_1}{[H^+]} + \frac{k_1 k_2}{[H^+]^2}\right) \ . \tag{16}$$

Then, we can find the concentration of hydrogen ions at a specific time solving the quadratic of

$$[H^+]^2 + [H^+]k_1(1 - \frac{C_U}{Alk} + k_1 k_2 \left(1 - \frac{2C_U}{Alk}\right) = 0 \tag{17}$$

where we take the positive root from the quadratic equation to be our hydrogen concentration.

The ability to store carbon decreases significantly as the pH increases. In theory, the carbon storage changes could as the heat of the ocean increases because of an decrease of solubility of CO_2 and increase of the disassociation constants, but these are much less than the effect that acidity on the ocean. This whole ocean carbon chemistry and flux can be represented with

$$\frac{dC_A}{dt} = -k_a C_A + k_a \frac{k_H}{\delta_a \Lambda} C_U + E(t) \ , \tag{18}$$

$$\frac{dC_U}{dt} = k_a C_A - k_a \frac{k_H}{\delta_a \Lambda} C_U - k_d C_U + \frac{k_d}{\delta_d} C_L \ , \tag{19}$$

$$\frac{dC_L}{dt} = k_d C_U - \frac{k_d}{\delta_d} C_L \ . \tag{20}$$

Ocean Carbon Store Parameters

Parameter	Value	Unit	Description
k_1	8.00×10^{-7}	mol/kg	disassociation constant
k_2	4.63×10^{-10}	mol/kg	disassociation constant
k_a	0.2	yrs $^{-1}$	turnover time for upper ocean
k_d	0.05	yrs $^{-1}$	turnover time for deep ocean
k_H	1.23×10^3		Henry's constant
Alk	767.0$\star$	GtC	alkalinity of the ocean
δ_d	50		ratio between upper and lower ocean
δ_a	solved for		ration between upper ocean and atmosphere
AM	1.77×10^{20}	moles	moles of the atmosphere
OM	7.8×10^{22}	moles	moles of the ocean

Table 2: From Glotter et al (2014). These are the values used to calculate the carbon cycle between the layers of the ocean and the atmosphere. Rows without units are unitless values. In our model, we convert all masses (GtC) to moles. Parameters k_1 and k_2 were converted to mole fraction by multiplying by 18/1000. ($\star$) We raised the alkalinity parameter by a factor 1.02 to better match pre-industrial CO2 uptake rates. This is still within the reported experimental range for ocean alkalinity.

2.3 Radiative Forcing

Radiative forcing (RF) is calculated for each greenhouse gas using the equations provided in the IPCC's assessment's fifth assessment report [17]. Radiative forcing due to CO_2 has a log-linear temperature response to excess carbon past pre-industrial conditions (C_0). CH_4 and N_2O have interacting RF due to infrared band overlap [16] reflected in the IPCC's formulas in the AR5 Table 8.SM.1 [17]. Formulas for RF are as follows :

$$\Delta N_{\mathrm{CO_2}} = \alpha \times \ln\left(\frac{C}{C_0}\right) \text{ where } \alpha = 5.35 \tag{21}$$

$$\Delta N_{\mathrm{CH_4}} = \alpha \times (\sqrt{M} - \sqrt{M_0}) - (f(M, N_0) - f(M_0, N_0), \text{ where } \alpha = 0.036 \tag{22}$$

$$\Delta N_{\mathrm{N_2O}} = \alpha \times (\sqrt{N} - \sqrt{N_0}) - (f(M_0, N) - f(M_0, N_0), \text{ where } \alpha = 0.12 \tag{23}$$

$$f(M, N) = 0.47 \times \ln[1 + 2.01 \times 10^{-5}(MN)^{0.75} + 5.31 \times 10^{-15} M(MN)^{1.52}] \tag{24}$$

$$\tag{25}$$

C, M, and N refer to current atmospheric concentrations of CO_2 in ppm, CH_4 in ppb, N_2O in ppb respectively. C_0, M_0 and N_0 refer to concentrations at 1750. The α term is the radiative forcing coefficient with units of $\frac{W}{m^2}$ and varies with each equation as indicated .

We also include differential equations for CH_4 and N_2O concentrations as a function of emissions and a fixed decay rate to reflect their atmospheric perturbation lifetimes as given by the IPCC [17]. We assume CO_2 does not decay from the atmosphere for the timescales considered because of its status as a millennial gas, but it cycles into various ocean and terrestrial stores as described by the carbon cycle. The changes in CH_4 and N_2O are represented by

$$\frac{d\mathrm{CH_4}}{dt} = E_{anthro} + E_{bio} + E_{pf} - \frac{\mathrm{CH_4}}{\nu_1} \tag{26}$$

$$\frac{d\mathrm{N_2O}}{dt} = E_{anthro} - \frac{\mathrm{N_2O}}{\nu_2}. \tag{27}$$

2.4 Temperature Response

Our model uses a two box temperature response model described by Pierrehumbert et al. (2014) [18]. This gives an accurate temperature response based on historical atmospheric concentrations of greenhouse gases and for projected emission streams (see 3).

Lifetime of Radiative Forcers

Variable	**Value**	Unit	**Description**
ν_1	12	year	lifetime of CH_4
ν_2	114	year	lifetime N_2O

Table 3: These perturbation lifetimes are the approximations used in the model. The lifetime for CH_4 is varied and does depend on atmospheric conditions. In the differential equation, the rate is held constant.

We use T_{mix} to describe the temperature perturbation of the upper or mixed layer of the ocean. This model uses the mixed ocean layer temperature as a proxy for Earth surface temperature because ocean temperatures largely dictates surface temperature. T_{deep} represents the temperature of the deep ocean. The model demonstrates the heat transfer between the two layers. We use μ to represent the heat capacity of each layer. The model uses γ for the heat transfer coefficient between the mixed and deep layers, and the $\hat{\lambda}$ for the climate sensitivity parameter, both in units of $\frac{W}{m^2 K}$. Temperature changes are driven by the change in radiative forcing, ΔN. The radiative forcing for each greenhouse gas is calculated and added together as a net ΔN, and we get the following:

$$\mu_{mix}\frac{dT'_{mix}}{dt} = -\hat{\lambda}T'_{mix} - \gamma(T'_{mix} - T'_{deep}) + \Delta N(t) \tag{28}$$

$$\mu_{deep}\frac{dT'_{deep}}{dt} = \gamma(T'_{mix} - T'_{deep}) \tag{29}$$

Temperature Response Parameters [18]

Parameter	**Value**	**Description**
μ_{mix}	3.154×10^8 J m^{-2} K^{-1}	heat capacity of mixed layer
μ_{deep}	6.307×10^9 J m^{-2} K^{-1}	heat capacity of deep ocean
$\hat{\lambda}$	1.2 W m^{-2} K^{-1}	climate sensitivity parameter
γ	1.2 W m^{-2} K^{-1}	heat transfer coefficient

Table 4: Temperature response parameters come from Pierrehumbert et al. 2014. In the implementation of the model, we converted γ and $\hat{\lambda}$ from watts to joules per year.

This two box ocean temperature response model represents the temperature dynamics of the upper mixed layer and the deep ocean given their different heat capacities.

2.5 Permafrost Feedback

A permafrost feedback is included in our model, as it is one of the major short term climate feedbacks. Figure 2 shows the how a portion of carbon in the permafrost becomes vulnerable as permafrost melts. This now vulnerable pool is subject to decomposition by microbial activity and thus emitted into the atmosphere as CO_2 or CH_4 . A portion of the permafrost carbon is considered fixed or "passive", as it is non-labile and will not be released during the timescales of our study. We make the assumption that the extent of the permafrost decreases linearly with increase of global mean temperature and that carbon content of the permafrost is spatially homogeneous [12].

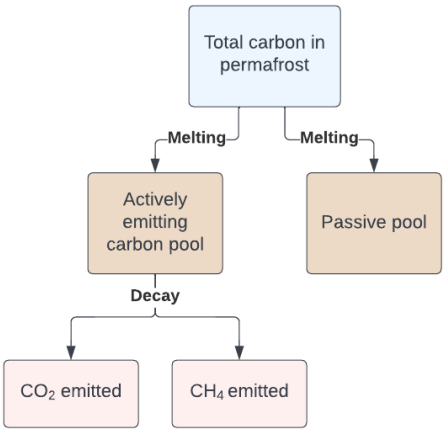

Figure 2: Permafrost sub-model schematic. Our first box of the permafrost module is the total carbon in the permafrost (C_{PF}, see equation (32)). As permafrost melts, soil is exposed. In the exposed soil, there is an actively emitting labile carbon pool (L_C and L_M, see equations (35) and (36)), and a passive or non-labile carbon pool. From the actively emitting carbon pool, carbon is released as CO_2 or CH_4 in constant proportion.

We follow the logic of Kessler's model but adapt into differential equation form [12]. The total carbon in the permafrost is C_{PF}. L_c and L_m combine to form the actively releasing labile carbon pool, where L_c is the proportion that is destined to b CO_2 , and L_m is the proportion that is be emitted as CH_4 . Together, they represent the labile portion of the pool of carbon that is now vulnerable due to a decrease in permafrost extent. L_c and L_m each have their own emission stream $E(t)$. These pools are assumed to be 0 when initializing the model at year 2010. The proportion of carbon that is emitted as CO_2 or CH_4 is determined by the proportion parameter ω.

We describe the intact frozen carbon in the permafrost as the total carbon pool at initial time t_0 times the proportion of the the permafrost left (PF_{extent}):

$$C_{frozen} = C_{PF}(t_0)PF_{extent}(t). \tag{30}$$

We describe the extent of permafrost at time t as follows:

$$PF_{extent}(t) = 1 - \beta \times (T(t) - T(t_0)), \tag{31}$$

where the permafrost extent decreases linearly with rise in global mean temperature (T) above an equilibrium temperature ($T(t_0)$)[12]. In our model, we use the temperature at year 2010 as $T(t_0)$, while Kessler uses the temperature at the year 2000 as t_0, so our model slightly underestimates melting. Additionally, the model does not allow C_{PF} to increase by the permafrost refreezing; it is unable to capture lost CH_4 and CO_2 by cooling of the Earth's temperature.

As temperature increases, the extent of the permafrost decreases, and there is newly thawed soil that is now vulnerable to microbial decomposition. We represent this this decomposition as exponential decay [12].

The loss of carbon from the labile pool is represented by the exponential decay term $-\frac{1}{\tau}$. The carbon that has decayed from the permafrost is then added into our emissions stream. This is the same for the active labile carbon pool being emitted as methane, because it is the remaining proportion (ω), and it shares the same decay rate $-\frac{1}{\tau}$.

The Kessler equations adapted into differential form are represented as [12]

$$\frac{dC_{PF}}{dt} = C_{frozen}(t) - C_{PF} = \rho : \quad \rho \leq 0 \tag{32}$$

$$\frac{dL_C}{dt} = -\rho \times (1-\eta) \times (1-\omega) - \frac{1}{\tau} L_C \tag{33}$$

$$\frac{dL_M}{dt} = -\rho \times (1-\eta) \times \omega - \frac{1}{\tau} L_M \tag{34}$$

$$E_{PF\ C}(t) = \frac{1}{\tau} L_C \tag{35}$$

$$E_{PF\ M}(t) = \frac{1}{\tau} L_M \quad . \tag{36}$$

Parameter	Value [12]	Description
C_{PF}	1035 GtC	total GtC in the permafrost
τ	70 yrs	e-folding time for decomposition
β	0.172	coefficient for permafrost melt rate
η	40 %	portion of non-labile carbon
ω	2.3 %	portion of carbon released as methane

Table 5: Permafrost parameters (Kessler et al., 2017)

Summary of Atmospheric Carbon

With the permafrost emissions added, we generalize our atmospheric carbon pool dynamics with:

$$\frac{dC_A}{dt} = E_{anthro} + E_{PF} + E_{LC} + F_T + F_O, \tag{37}$$

where E_{anthro} is fossil fuel emissions, E_{PF} is the emissions from the permafrost, E_{LC} is land use emissions, F_T is the flux of carbon between the terrestrial stores from net primary productivity and respiration ($-NPP + RH_{det,soil}$ see equations (1), (2) and (3)) , and F_O is the flux of carbon into the oceanic sinks ($-k_a C_A + k_a \frac{k_H}{\delta_a \Lambda} C_U$ see equations (18)).

2.6 Validation and Initial Conditions

We begin by burning in the model using the atmospheric CO_2 concentration at 1750 levels and running the model for a few thousand years to allow the levels of carbon in the ocean and terrestrial stores to stabilize. We then use these stabilized values as our initial conditions for 1750 for the vegetation, detritus, soil, upper ocean and lower ocean boxes.

We then checked our model's temperature response and carbon cycle modules using historical data [24]. Our initial conditions for 1750 are given in Table 6. We drove the model from 1750 to 2010 using historical emissions data from the AR5 report [24], allowing our model to calculate atmospheric CO_2 concentrations based on its carbon cycle modules (Figure 3 (b)). The model also calculated temperature from the radiative forcing of the amount of CO_2 in the atmosphere (Figure 3 (a)), which shows a reasonably similar temperature result for 2010 [1].

To get our actual conditions in the year 2010, we used actual parts per million data of CO_2 in the atmosphere to calculate the radiative forcing instead of the emissions streams [24]. After running the model to 2010, we took the carbon content of our upper ocean, lower ocean, vegetation, detritus, and soil boxes, along with the temperatures, as the initial conditions for projecting the model forwards.

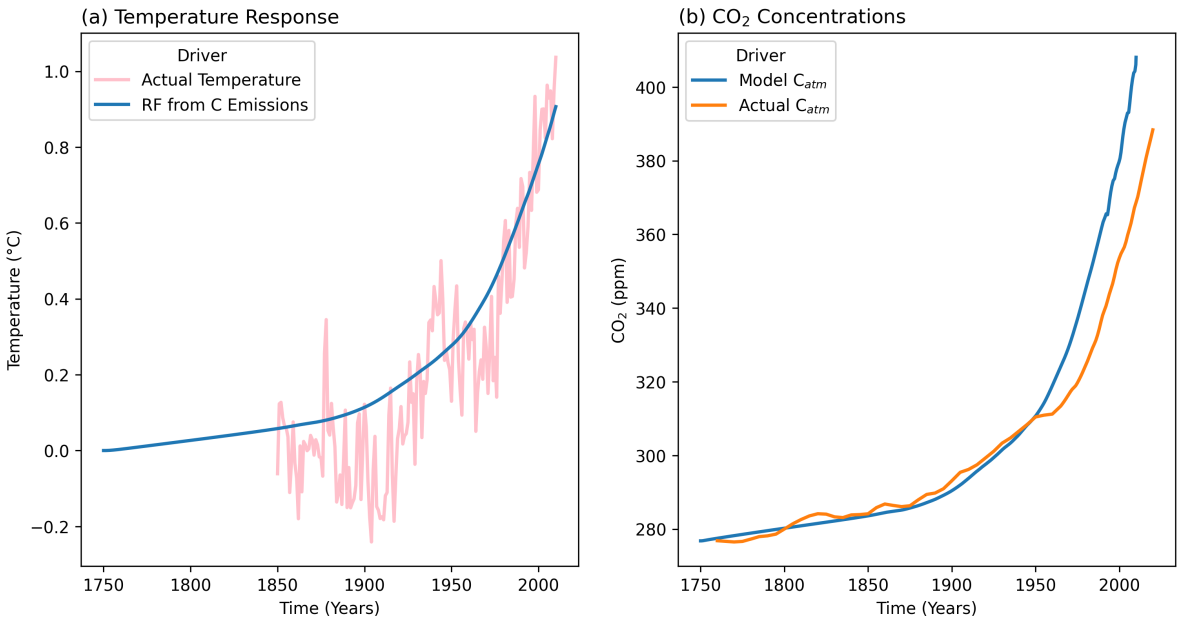

Figure 3: Validation of model against historical temperatures and atmospheric CO_2 concentrations. (a) shows historical temperature data in pink, and our modeled temperature response driven by radiative forcing from carbon emissions after our model adjusts for fluxes between the atmosphere and other boxes. (b) shows atmospheric carbon concentrations from actual historical data in orange, versus our modeled carbon concentrations in blue.

Variable	Unit	Year 1750	Year 2010	Description	Notes
T_{mix}	$C°$	0	0.81	surface temperature	
T_{deep}	$C°$	0	0.22	lower ocean temperature	
C_A	GtC	587.92	824.91	carbon in atmosphere	Glotter et al. 2014
C_U	GtC	725.39	740.35	carbon in upper ocean	
C_L	GtC	36263.18	36310.28	carbon in lower ocean	
C_v	GtC	500	536.95	carbon in vegetation	Hartin et al. 2016
C_D	GtC	55.29	59.73	carbon in detritus	
C_S	GtC	1808.82	1767.11	carbon in soil	
CH_4	ppb	N/A	1798.0	methane concentration	EEA 2019 [2]
N_2O	ppb	N/A	323.7	nitrous oxide concentration	
C_{pf}	GtC	N/A	1035	carbon (frozen) in permafrost	Kessler et al. 2017
L_C	GtC	N/A	0	labile carbon	
L_M	GtC	N/A	0	labile methane (as carbon)	

Table 6: Initial conditions for the year 2010, either found by driving the model with historical atmospheric concentration data or from other works (reference given in this case). These are the initial conditions used for our projections.

2.7 Future Emission Scenarios

To determine the impact of methane mitigation strategies on permafrost climate feedbacks, we projected our model forward using the AR5's extended RCP 2.6, 4.5, and 6.0 CO_2 and N_2O emission streams [15]. We combine these given RCP CO_2 and N_2O emission streams with our own calculated CH_4 emission stream based on different annual reduction plans. All CH_4 emission streams for all scenarios start at 2010 with 330 Mt of CH_4 emitted that year, and are extended out until 2300. To examine the impact of just the rate of phase-out, not magnitude, we take our initial value of 330 Mt and reduce it by a given percentage annually until it reaches the same "floor" level of the given RCP.

For example, RCP 2.6's projected methane emission stream reduces from 330 Mt/year to 142 Mt/year by 2100, where it then remains until 2300. Therefore, we take 330 Mt, and reduce it by a given percentage annually until it reaches 142 Mt and then hold that level constant. We can then compare varying rates of phase-out to the given "baseline" RCP scenario. For reference, the floor value for RCP 4.5 is 266 Mt/year, and for RCP 6, 252 Mt/year.

To compare magnitude of phase-out, we take our projected methane emission streams to a lower final value than the RCP.

3 Results

We generated a temperature time series for all scenarios. We projected forward the "baseline" unaltered RCP emission scenarios then ran the same scenario again with the permafrost module in effect. This gave a significant change in temperature from the baseline RCP scenario and can be seen in Figure 4. Each RCP scenario had two main temperature projections, with one slightly higher with the permafrost feedback module in effect.

We also compared each RCP scenario with a rapid 10% annual methane emission reduction plan, shown by the dashed lines in Figure 4. The 10% reduction plan reached the same target emission rate as the respective RCP and was then held constant. For example, we compared the baseline RCP 2.6 with our RCP 2.6 with the 10% annual methane phase-out; both reached the same final target of Mt CH_4 emitted each year (142 Mt CH_4). Both reached and then remained at this target level of 142 Mt CH_4 emitted annually through 2300. This comparison was made with and without the permafrost feedback. A 10% phase-out is considered very accelerated, and the target emission rate was reached within less than 5 years.

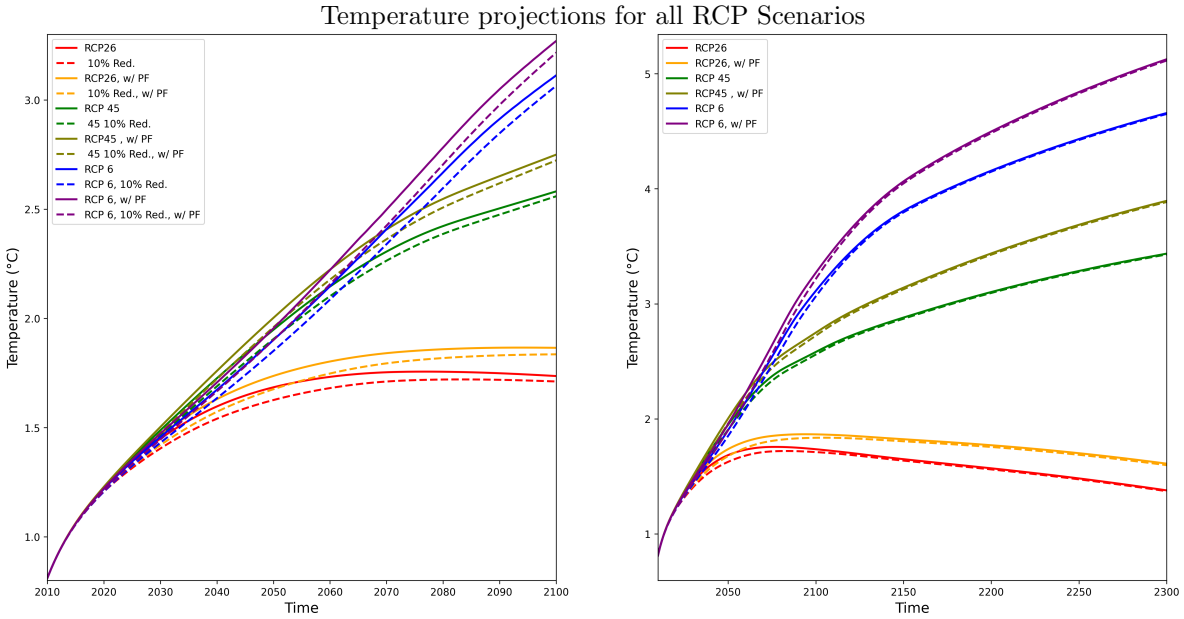

Figure 4: Temperature responses for RCP 2.6, 4.5, and 6 emission scenarios, with and without a permafrost feedback effect, (a) from 2010-2100 and (b) from 2010-2300. Dashed lines show a 10% annual methane phase-out for the given scenario while solid lines show the baseline RCP scenario. Greatest differences in temperature between baseline RCP and 10% annual phase-out are seen before 2100. From 2100-2300, the projections with and without the rapid 10% methane reduction plans are largely the same, with or without a permafrost feedback.

Year	RCP 2.6	RCP 4.5	RCP 6
2100, without PF (°K)	1.73	2.60	3.16
2100, with PF (°K)	1.86	2.77	3.31
Difference (°K)	0.13	0.17	0.15
% Difference	7.5%	6.5%	4.7%
2300, without PF (°K)	1.38	3.14	4.66
2300, with PF (°K)	1.61	3.9	5.13
Difference (°K)	0.23	0.46	0.47
% Difference	16.7%	13.4%	10.1%

Table 7: Temperature perturbation at year 2100 and 2300, with and without the permafrost feedback effect under different RCP scenarios. Note that these results do not include accelerated methane phase-outs.

We compared our accelerated methane mitigation plans to the RCP's standard methane projections. For each RCP scenario, we used the IPCC's CO_2 emission projections, shown in gigatonnes of carbon in Figure 5 (a), (c), and (e). We included each RCP's given N_2O emission projections to accurately calculate methane's radiative forcing, taking into account the band overlap explained in section 2.3 We then compared the results of our methane mitigation plans with the results from running the unaltered RCP scenario. We used a 5% and 10% annual methane reduction rate to compare to RCP 2.6, as a 1% annual reduction rate was slower than their projection. For RCP 4.5 and 6, we used a 1% and 10% annual methane reduction rate, seen in Figure 5 (b), (d), and (f). Figure 5 shows the net emissions used in our projections from 2010 to 2300 as we vary CH_4 reduction rates and use the given RCP CO_2 emission projection.

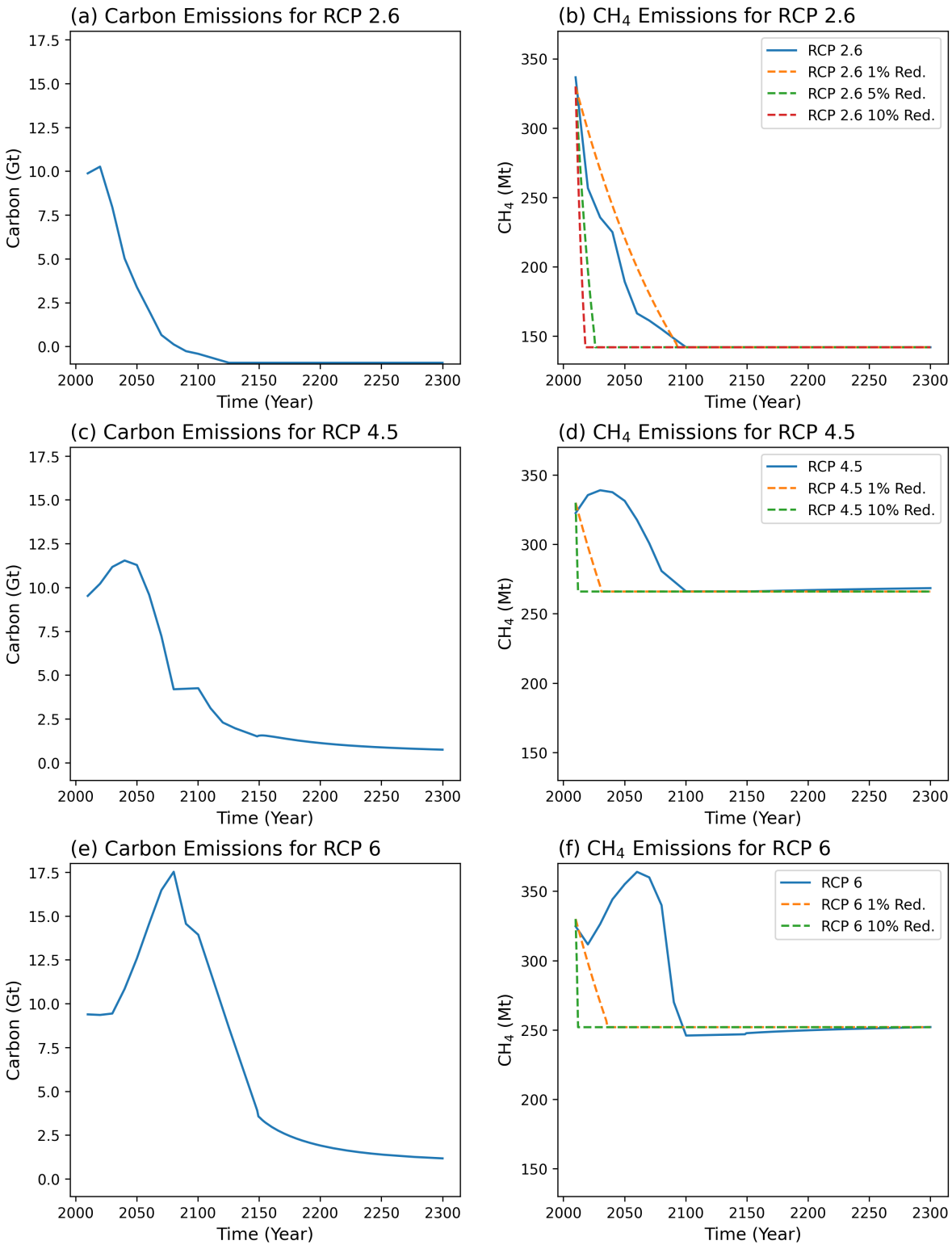

Figure 5: Emissions streams for all RCP scenarios and RCP scenarios with accelerated methane phase-out. Solid lines represent baseline RCP scenarios, while dashed lines represent our imposed methane mitigation scenarios. Figures show net emissions per year. In Figures (a), (c), and (e), carbon emissions in gigatonnes are shown, as given by the RCP projection. In Figures (b), (d), and (f), CH_4 emissions in megatonnes are shown for the baseline RCP and our reduction scenarios.

3.1 RCP 2.6

We began by running the baseline RCP 2.6 with unaltered emission streams for CO_2 and CH_4 out to year 2300, without the permafrost module in effect. We then ran the model again with the same emission streams, but with the permafrost module in effect (see Figure 6 (a)). The final temperature perturbation at year 2300 reaches 1.38°C above pre-industrial levels. With the permafrost feedback, temperature reached 1.61°C, a difference of 0.23°C. We found there to be 97.7 GtC emitted from the permafrost at year 2300.

Using the RCP 2.6 CO_2 emission scenario, we reduced anthropogenic methane from 330 Mt in 2010 by 5% or 10% annually until we reached a constant emission rate of 142 Mt of CH_4 per year. 142 $MtCH_4$ per year was used as the target emission rate as it is consistent with lowest value for the RCP2.6 (i.e., RCP 2.6 projection reaches a minimum or "target" level of 142 $MtCH_4$ per year at 2100 and remains there onward through year 2300). Therefore, we only differed from RCP 2.6 in how long it took to reach that target. We used two highly accelerated methane reduction plans, 5% and 10% so as to phase out faster than the RCP 2.6, as the baseline RCP 2.6 is already an accelerated mitigation scenario for all greenhouse gases.

We found that the rate of methane mitigation had a negligible effect on temperature at 2300, but had an effect before 2100. The largest difference in temperature occurs at 2050, where there is a 0.06°C difference between the standard RCP 2.6 scenario compared to the 10% phase-out.

At the year 2300, 97.7 GtC was emitted from the permafrost under baseline RCP 2.6. 95.3 GtC was emitted under a 5% methane reduction plan, while 94.4 GtC was emitted with a 10% methane reduction plan. This may be because under RCP 2.6's aggressive CO_2 mitigation projection, CH_4 emission mitigation has a relatively stronger effect. We find that there is less sparing of permafrost while running other RCP scenarios.

Atmospheric concentrations of CO_2 are largely the same for all scenarios, and atmospheric concentrations for CH_4 reflect our differing reduction strategies (see Figure 6 (c) and (d).

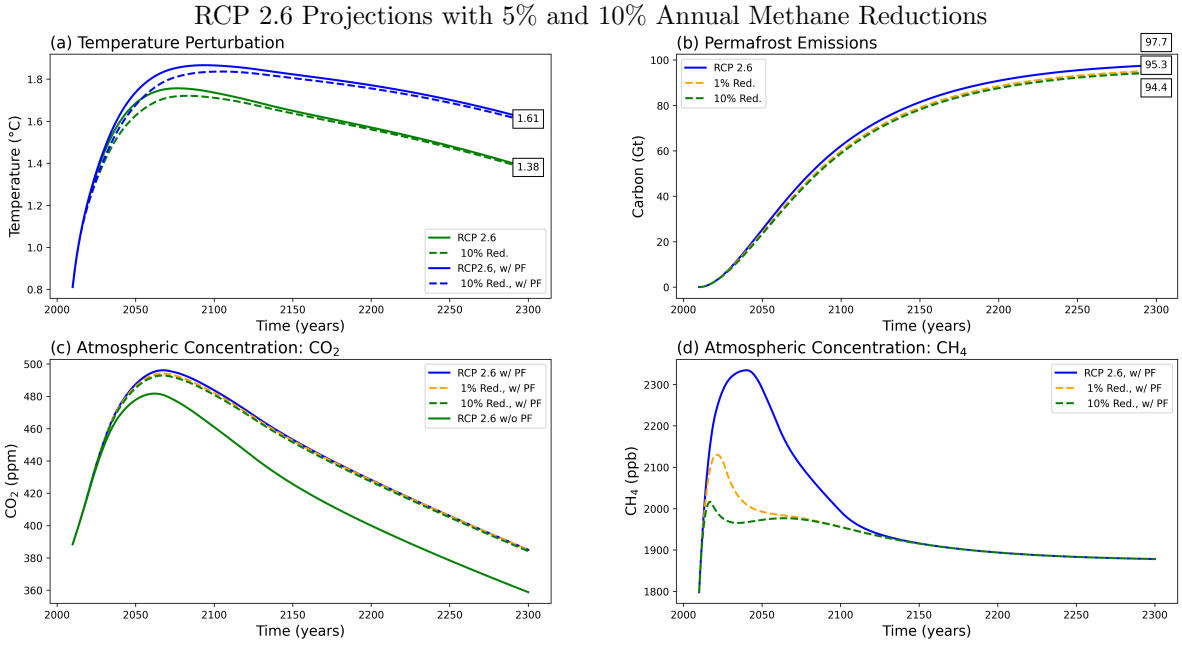

Figure 6: Results for 5% and %10 methane phase-out strategies using RCP 2.6 CO_2 scenario. Dotted lines represent our imposed methane mitigation scenarios, while solid lines represent the "baseline" RCP 2.6 scenario. We look at temperature perturbation at the year 2300 in (a), permafrost emissions at the year 2300 in (b), and atmospheric concentrations of CO_2 and CH_4 in (b) and (c).

3.2 RCP 4.5

We evaluated the impact of rate of mitigation under the RCP 4.5 emission scenario using the same procedures.

First, we looked at temperature perturbation of the baseline RCP 4.5 scenario with and without a permafrost feedback effect. We ran the with the baseline RCP 4.5 emission scenario to the year 2300 without the permafrost module and found temperature was 3.44 °C. Running the baseline scenario again with the permafrost module, the temperature perturbation was 3.9°C (see table 7). We found there to be 277.8 GtC emitted from the permafrost by year 2300.

The target value of CH_4 emissions per year was set to 266 $MtCH_4$ per year, as consistent with the target level from the RCP 4.5. The RCP 4.5 reaches 266 $MtCH_4$ per year at year 2100 and remains constant through year 2300.

We performed a 1% or 10% methane mitigation plan to take emissions from 330 to 266 Mt CH_4 per year. In Figure 7 (d), the atmospheric concentrations of CH_4 are shown for the different scenarios. The mitigation plans reduced atmospheric methane concentrations compared to the baseline RCP before year 2100. After the year 2100, atmospheric concentrations remained the same between all scenarios, as expected since our reduction plans meet the same target value as the RCP 4.5.

The 1% and 10% phase-out schemes produce effectively the same final temperature perturbation, although there was a transient temperature difference before year 2100 (see Figure 4). The temperature projections converged and were virtually identical by the year 2300 (see Table 7).

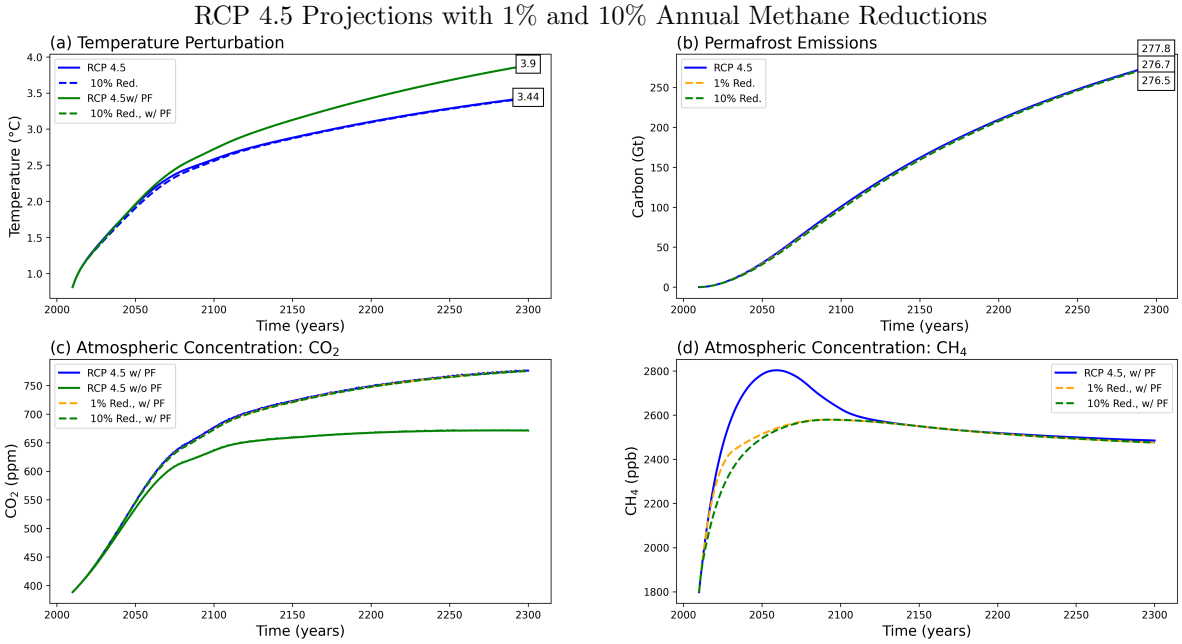

Figure 7: RCP 4.5 results for 1% and %10 reduction to annual methane emissions. (a) shows final temperature perturbation with and without the permafrost feedback module in effect, with the dashed line showing the 10% reduction scenario. (b) shows the permafrost emissions in gigatonnes of carbon for the baseline RCP scenario compared to the 1% and 10% reduction plans.(c) and (d) show atmospheric concentrations of CO_2 and CH_4 respectively over time.

3.3 RCP 6

We evaluated methane mitigation plans compared with baseline RCP 6 projections (Figure 8). Temperature perturbation at the year 2300 without the permafrost module was 4.66 °C, and 5.13 °C with the permafrost module (see Table 7). We found there to be 392.9 GtC emitted from the permafrost at the year 2300.

The target methane emission rate for RCP 6 was 252 $MtCH_4$ yearly. Our methane mitigation scenarios went from 330 $MtCH_4$ emitted in year 2010, reduced by 1% or 10% annually until reaching 252 $MtCH_4$ and were then held constant for future years.

The temperature trajectories in Figure 8 (a) were, in the long term, consistent between the baseline RCP projection and the imposed methane mitigation scenarios. There were significantly lower atmospheric concentrations of methane from the 2010-2100 under the mitigation strategies, however, this did not effect temperature projections or significantly impact permafrost emissions. Permafrost emissions were 1.7 GtC lower in the year 2100 from the 10% mitigation scenario, compared to the baseline RCP 6.

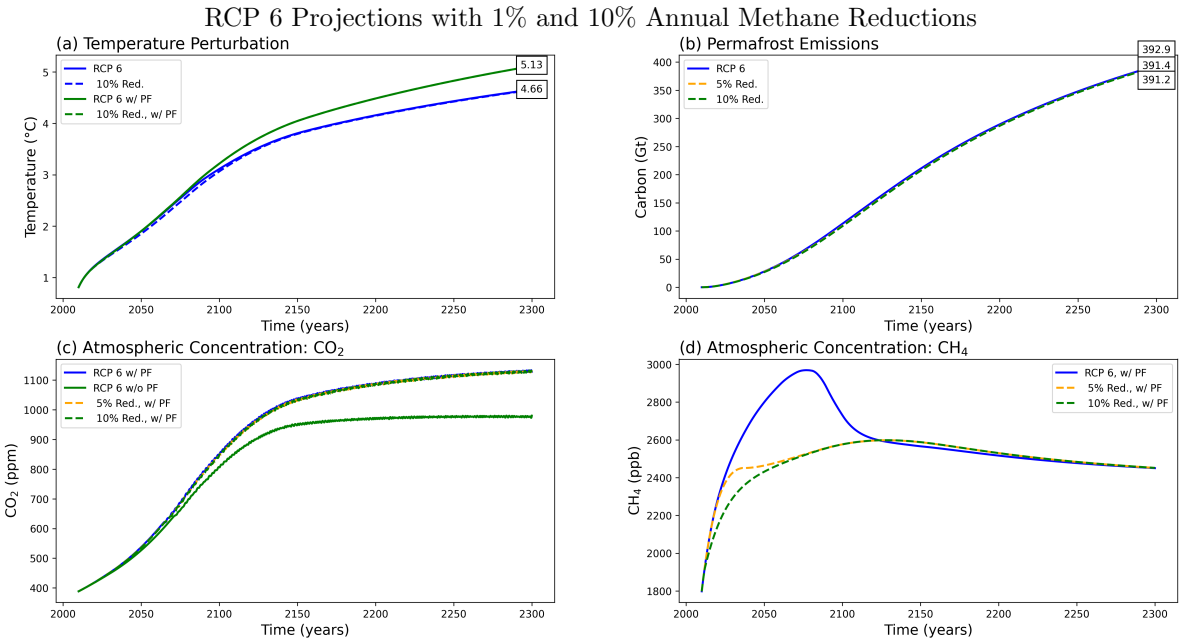

Figure 8: RCP 6 results for 1% and %10 methane reduction rates. (a) shows temperature perturbation at year 2300, with and without a permafrost feedback effect. Dashed lines denote an imposed methane reduction strategy, while solid lines represent the baseline RCP projection. (b) shows permafrost emissions in gigatonnes of carbon with a difference of 1.7 GtC at the year 2300 between the baseline RCP projection and the 10% methane mitigation plan.(c) and (d) show atmospheric concentrations of CO_2 and CH_4 respectively.

3.4 Final Magnitude Versus Rate of Mitigation

Finally, we directly compared the effect magnitude and rate of methane mitigation on final temperature perturbation at the year 2300 while including the permafrost feedback module. We used the RCP 4.5 scenario for this comparison. We ran the model with methane reduction rates between 0.1% and 10% to targets between 125 Mt CH_4 and 275 Mt CH_4 per year to obtain a temperature perturbation at the year 2300.

Importantly, reduction rates below 0.5% never reached the low end target of 125 Mt CH_4 emissions per year at 2300. If emissions were reduced by less than 0.5% annually, there was not enough time from 2010 to 2300 to take emissions levels from 330 Mt CH_4 per year to 125 Mt CH_4 per year. For example, with a reduction rate of 0.1%, there was still 246 Mt CH_4 being emitted at the year 2300, and with 0.25% reduction rate, there was 160 Mt CH_4 emitted at 2300. This accounts for the difference in temperature perturbation at the year 2300 between the rates of 0.1 and 0.25% and the higher rates which converge to 3.7°C.

We saw a linear relationship between target methane annual emissions and final temperature perturbation. Rates that were able to meet the target of 125 Mt CH_4 per year (1%-10% reductions annually) all show a strong cluster around 3.7°C final perturbation. 0.5% reduction rate reached the target of 125 MtCH_4 per year at year 2300, however, it reaches this goal much closer to year 2300 than the more accelerated plans. Thus, the spread around 3.7°C can by greater emissions from a slower convergence to 125 MtCH_4 . Overall, magnitude of reductions proved to be more important than rate of reduction, provided the rate was fast enough to meet the target by year 2300.

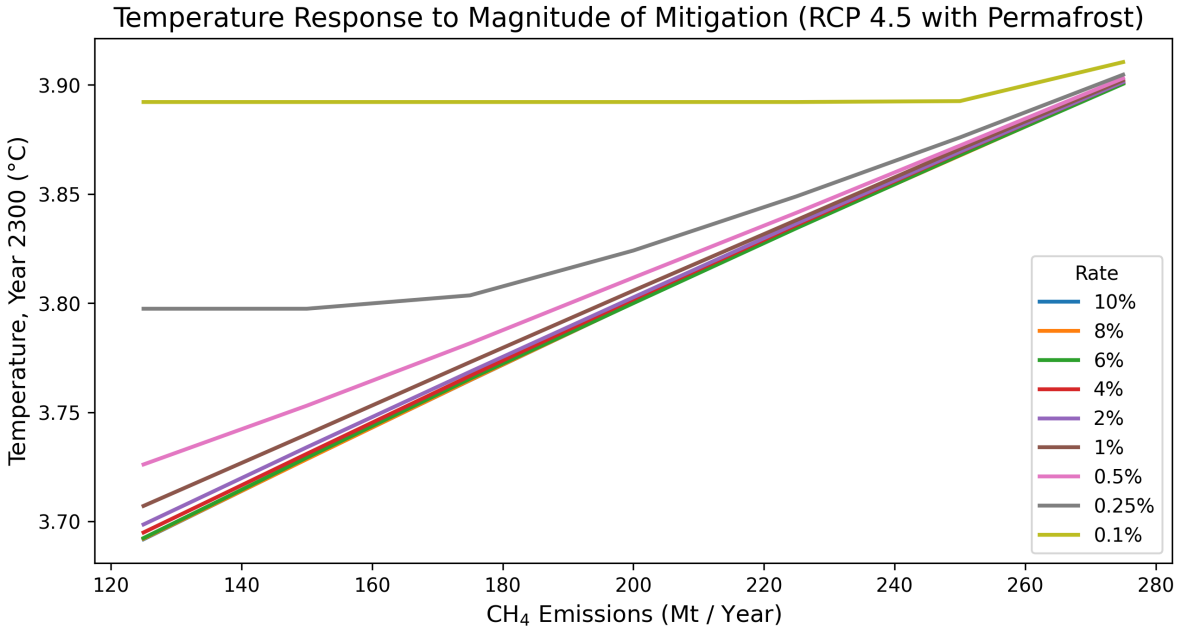

Figure 9: Comparing the impact of rates of mitigation to different target levels using RCP 4.5. Importantly, with a very slow annual mitigation rate below 1% each year (0.5%, 0.25%, 0.1%) the final target of 125 Mt CH_4 per year was not reached. The magnitude of mitigation shows a strong relationship to final temperature, with a 0.2°Celsius difference in temperature between 120 MtCH_4 and 275 MtCH_4 emitted per year.

Using RCP 4.5 with the permafrost feedback module, we then compared rate of methane mitigation to temperature perturbation at year 2300. When rates were below 0.5%, methane mitigation targets were not reached. Between 1% and 10% annual reduction in emissions, the temperature response is largely the same, shown by the horizontal lines. We saw the same temperature perturbation across 1%, 2%, 4%, 6%, 8%, and 10% annual reduction for each final mitigation target (125, 150, 175, 200, 225, 250, and 275 MtCH_4 /year). The final target mitigation level (assuming it was reached) determined the temperature perturbation.

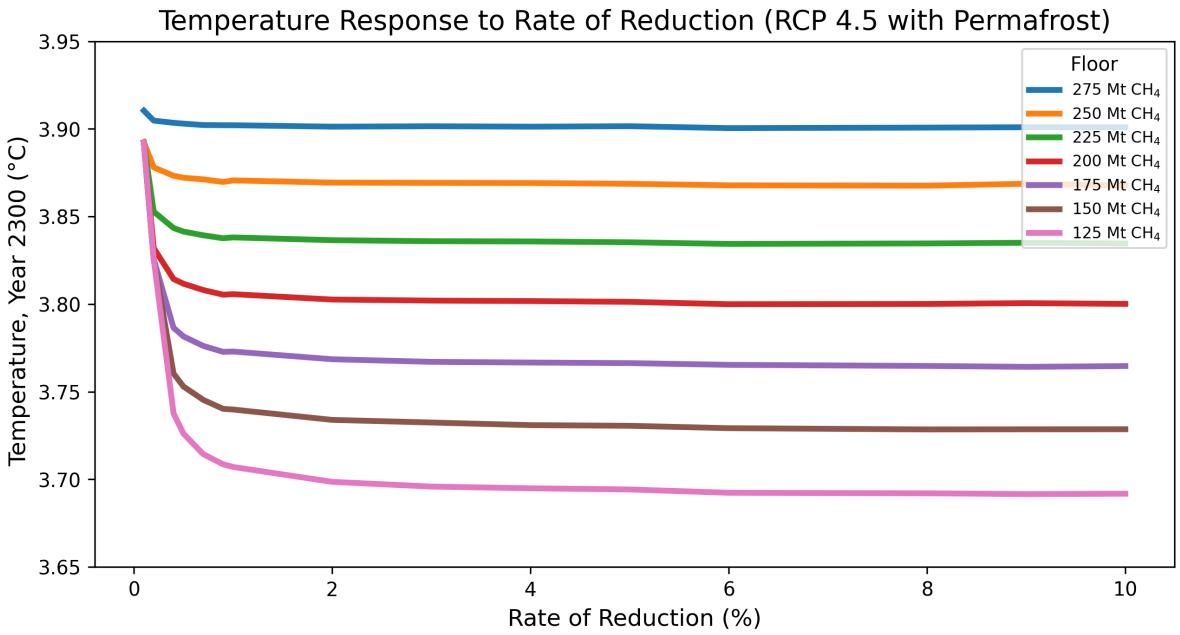

Figure 10: Rate of mitigation compared to temperature perturbation at the year 2300 using RCP 4.5. For rates of reduction below 1%, final mitigation targets are not met; therefore, temperatures are higher. For example, for mitigation to 125 Mt CH_4 annually, the rate of reduction must be over 1 percent each year to achieve this target. When target emission rates are reached, temperature is determined by the final mitigation target.

In summary, we compared rate of methane reduction against target mitigation level and temperature (Figure 11). We used the same ranges as previously, excluding 0.1% and 0.25% reduction rates here as they could not reach the target mitigation level by 2300. For the rates shown between 0.5% and 10%, temperature perturbation was equal at year 2300. We found temperature perturbation responded highly linearly to the magnitude of mitigation, and not rate of reduction.

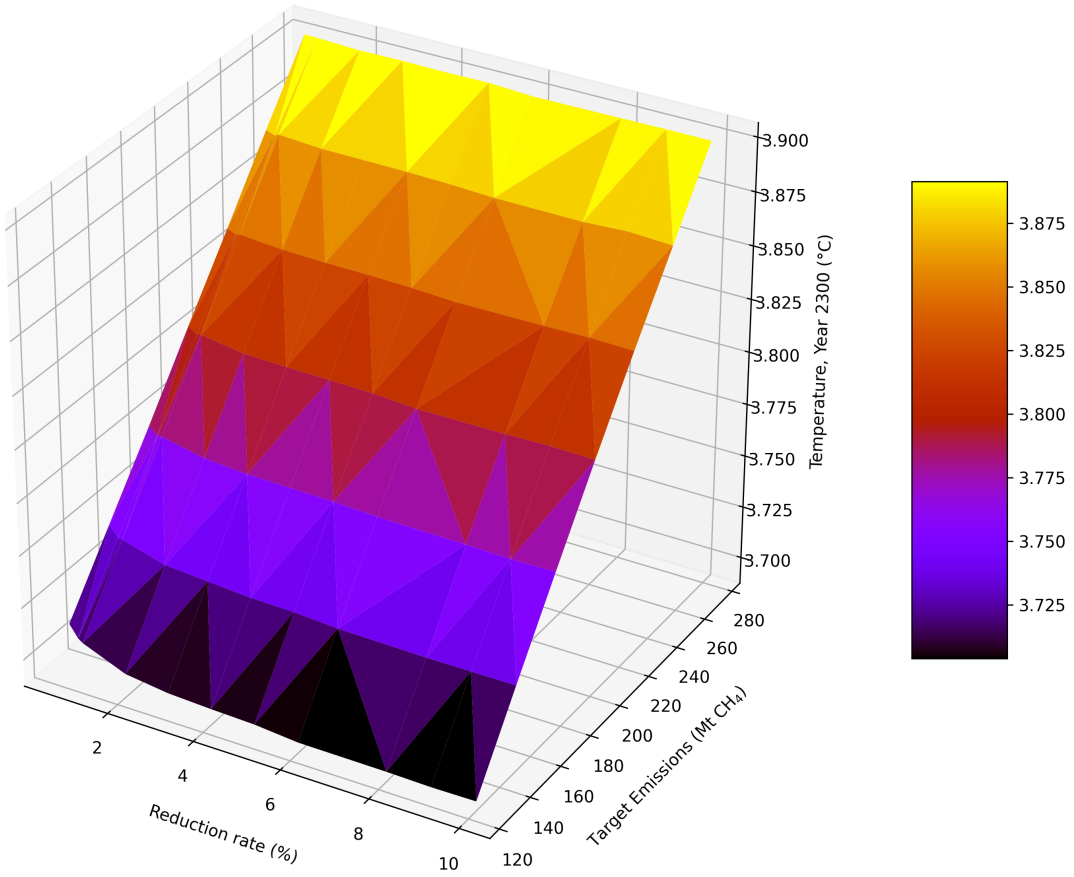

Figure 11: The effect of reduction rate and target emission level on temperature perturbation at year 2300. Reduction rates vary between 0.5% and 10% and target emission levels vary between 125 and 275 Mt CH_4 . Time span is from 2010 to 2300. CO_2 emission projection is from RCP 4.5.

4 Discussion

We developed and used our reduced complexity global Earth systems model to examine the long-term temperature response to methane mitigation rates in the presence of a permafrost feedback effect. We sought to clarify methane emission mitigation priorities. While CO_2 emission mitigation is critically urgent as CO_2 is atmospherically long-lasting and emissions will effect climate for thousands of years, methane mitigation priorities are much less clear. It is widely agreed that methane emissions should be reduced, but how quickly must we act? Methane is atmospherically short lived, but because of its global warming potential of 28 times that of CO_2 over a 100 year span, does it warrant an accelerated phase-out [17]? Could its powerful warming cause accelerated permafrost thaw, warranting its mitigation more attention?

Looking at the permafrost feedback alone without methane mitigation, we found a significant difference in temperature perturbation. At year 2100, we saw a difference of 0.13-0.15°K (4.7-7.5%) between all RCP scenarios, and at 2300, a difference of 0.23-0.47°K (10.1-16.7%) (see Table 7). We found the permafrost feedback to be a significant positive feedback that should be included in future climate modeling.

We then generated accelerated methane mitigation scenarios to compare their long-term temperature perturbation with the IPCC's baseline RCP scenarios. We used the same methane emissions targets as the RCP scenario, and reduced anthropogenic methane emissions by 1%, 5% or 10% annually until we reached that target. We found that mitigating methane at an accelerated rate did not prevent long term permafrost thaw or have a long term effect on temperature perturbation.

We found that long temperature perturbation was largely determined by the magnitude of methane mitigation, not the rate of annual reduction. Provided the phase-out of methane was fast enough to reach the target level, the rate of annual reduction had a negligible effect. Of course, to reach a lower target level, the rate of mitigation had to be sufficiently fast to hit the target on a relevant timescale; in the case of our model, that had to be before the year 2300. Because methane is short lived greenhouse gas with an atmospheric lifetime of approximately 12 years, ultimately the greatest factor was how low annual methane emission levels could be brought to.

While methane emissions must be mitigated, we found negligible long-term benefits to implementing a highly accelerated methane phase-out. When we reduced methane emissions to their target levels within 10 years with a 10% annual reduction, we saw a slight difference in temperature this century (see Figure 4). This, however, was transient cooling and CO_2 ultimately determined the long term temperature course.

4.1 Model Limitations

Our reduced complexity model recreates carbon fluxes and changes in radiative forcing while demonstrating a reasonable permafrost response. Our model aims to show dynamics between anthropogenic emissions and permafrost thaw and decomposition, but it is not conclusively predictive. While the model reflects the behavior of the system well, some detail should be included in future works to make projections more accurate.

For the purposes the study, we included radiative forcing only from CO_2 , CH_4 , and N_2O . These were able to adequately recreate surface temperature in the year 2010 where we start our projections. In future work, other climate forcers such as black carbon, aerosols, halocarbons, ozone and other compounds should be included although they are not expected to make significant changes in the qualitative results, as historically, the cooling from aerosols has negated the warming from these other compounds.

The major source of uncertainty is permafrost modeling. While there is the most consensus on the total carbon stores in the northern hemisphere permafrost, there is great uncertainty regarding melting rates, microbial decomposition, and spatial heterogeneity. For example, our use of global mean temperature perturbation does not reflect regional temperature differences. One area of permafrost may thaw at a faster rate than another area due to these temperature differences. This unequal warming could also cause differing rates of microbial decomposition in different areas. As well, our model assumes permafrost thaw is a linear response to temperature increase. Another method of permafrost modeling uses a logarithmic scale where there is effectively "diminishing returns" of additional warming once the uppermost soil layers are thawed [27].

There is additional uncertainty regarding location of permafrost carbon stores– there may be areas of permafrost that have higher concentrations of carbon content than others, and more research is needed in permafrost mapping. A final concern is the rate of microbial decay, or "e-folding" time. Our permafrost model is sensitive to this parameter. We are using the constant value of 70 yr^{-1}, but the range of this value could be between 0-200 yr^{-1} and may be variable [12].

Another consideration may be the changing trends of methane-climate feedbacks in the coming decades [5]. There may be increasing levels of methanogenesis from wetlands and wildfires and a reduced methane atmospheric sink via hydroxyl radicals [5]. These trends are not included in our model, but, in practice, we would expect an overall increase in biogenic methane in the future due to increased temperatures and an overall decreased atmospheric sink. However, in our paper, we only consider a constant value for methane decay rate in the atmosphere and natural emissions without these factors.

4.2 Comparison to other works

Macdougall et al. (2012) used a modified version of the Earth System Climate Model (ESCM) and found temperature difference attributable to permafrost thaw at 2100 to be 0.1-0.8°C, estimated at 0.27°C (consistent across different emission scenarios) [14].

Crichton et al. (2016) added a permafrost-carbon module to the Earth System Model of Intermediate Complexity(EMIC), CLIMBER-2, and found increases of 10-40% of the maximum temperature change [6].

Burke et al. (2017) used the land surface model JULES (Joint UK Land Environment Simulator), along with ORCHIDEE-MICT (Organizing Carbon and Hydrology in Dynamic Ecosystems), modified to include permafrost carbon, coupled to the Integrated Model Of Global Effects of climatic aNomalies (IMOGEN), an intermediate-complexity climate and ocean carbon model. They found a difference of 0.2-12% of the maximum temperature change [4].

Woodard et al. (2021) used a permafrost implementation in Hector v.2.3pf and found approximately 0.2°C or 4–15% by 2100 across all RCP scenarios [27].

In comparison, we found between 0.13 and 0.15°C (4.7-7.5%) temperature perturbation attributable to the permafrost at 2100. This is on the low end but within the previously found range. We found a difference at 2300 (assumed maximum temperature change) of 0.23-0.47°C (10.1-16.7%) which is on the low range of Crichton et al. but on the high range of Burke et al. [4].

5 Conclusions

A benefit to an accelerated methane mitigation plan is that methane and CO_2 mitigation are coupled. As much of anthropogenic methane emissions are from fossil fuels (108-135 $MtCH_4$ per year), plans to move away from fossil fuels and mitigate CO_2 will also mean mitigating methane [11]. As Pierrehumbert et al. (2014) have argued, mitigating CO_2 immediately is of the utmost importance because of its long lasting climate effects, and methane mitigation is not a substitute [18]. Our research found that the extent of permafrost thaw was largely dependent on which RCP CO_2 emission projection we used and not the rate of methane mitigation (*although methane mitigation must still occur*). Bringing methane emission levels down to the lowest levels possible will play an important role in avoiding the climate boundary when done *in addition* to mitigating CO_2 . By bringing down the RCP 4.5 final methane emissions down to RCP 2.6 levels, there is a 0.22°temperature difference at 2300.

We see marginal long term benefit from rapid methane phase-out in relation to permafrost thaw. However, there is still a considerable short term benefit which may have effects on other sensitive feedbacks. Positive feedbacks, such as Amazon rainforest dieback, boreal forest loss, ice sheet melt, reduction in sea ice, etc., may amplify each other and have considerable effect on outcomes [13][19]. Inclusion of these other feedbacks and greater permafrost certainty would increase the confidence of the model.

Acknowledgements

We would like to thank Dr. Fabio Milner, Director of the Simon A. Levin Mathematical, Computational and Modeling Sciences Center (Levin Center), for giving us the opportunity to participate in the

Quantitative Research in the Life and Social Sciences program. We would also like to thank Co-Directors Dr. Abba Gumel and Dr. John Nagy for their efforts in planning and executing the program's instruction and activities. We also recognize the work of the many administrative staff and tutors who supported this effort. This research was conducted as part of 2022 QRLSSP at the Levin Center (MCMSC) at Arizona State University (ASU). This project has been partially supported by grants from the National Science Foundation (NSF Grant-DMS-1757968 and NSF Grant FAIN-2150492), the National Security Agency (NSA Grant H98230-20-1-0164), the Office of the President of ASU, and the Office of the Provost of ASU.

References

[1]

[2] *Trends in atmospheric concentrations of co2 (ppm), ch4 (ppb) and n2o (ppb), between 1800 and 2017*, European Environment Agency, (2019).

[3] M. Allen, O. Dube, W. Solecki, F. Aragón-Durand, W. Cramer, S. Humphreys, M. Kainuma, J. Kala, N. Mahowald, Y. Mulugetta, and et al., *Framing and context*, 2018: Framing and Context (Global Warming of 1.5°C), Global Warming of 1.5°C. An IPCC Special Report on the impacts of global warming of 1.5°C above pre-industrial levels and related global greenhouse gas emission pathways, in the context of strengthening the global response to the threat of climate change, sustainable development, and efforts to eradicate poverty (2022), p. 49–92.

[4] E. J. Burke, A. Ekici, Y. Huang, S. E. Chadburn, C. Huntingford, P. Ciais, P. Friedlingstein, S. Peng, and G. Krinner, *Quantifying uncertainties of permafrost carbon–climate feedbacks*, Biogeosciences, 14 (2017), pp. 3051–3066.

[5] C.-H. Cheng and S. A. T. Redfern, *Impact of interannual and multidecadal trends on methane-climate feedbacks and sensitivity*, Nature News, (2022).

[6] K. A. Crichton, N. Bouttes, D. M. Roche, J. Chappellaz, and G. Krinner, *Permafrost carbon as a missing link to explain co2 changes during the last deglaciation*, Nature Geoscience, 9 (2016), p. 683–686.

[7] P. Friedlingstein, M. W. Jones, M. O'Sullivan, R. M. Andrew, D. C. E. Bakker, J. Hauck, C. Le Quéré, G. P. Peters, W. Peters, J. Pongratz, S. Sitch, J. G. Canadell, P. Ciais, R. B. Jackson, S. R. Alin, P. Anthoni, N. R. Bates, M. Becker, N. Bellouin, L. Bopp, T. T. T. Chau, F. Chevallier, L. P. Chini, M. Cronin, K. I. Currie, B. Decharme, L. M. Djeutchouang, X. Dou, W. Evans, R. A. Feely, L. Feng, T. Gasser, D. Gilfillan, T. Gkritzalis, G. Grassi, L. Gregor, N. Gruber, O. Gürses, I. Harris, R. A. Houghton, G. C. Hurtt, Y. Iida, T. Ilyina, I. T. Luijkx, A. Jain, S. D. Jones, E. Kato, D. Kennedy, K. Klein Goldewijk, J. Knauer, J. I. Korsbakken, A. Körtzinger, P. Landschützer, S. K. Lauvset, N. Lefèvre, S. Lienert, J. Liu, G. Marland, P. C. McGuire, J. R. Melton, D. R. Munro, J. E. M. S. Nabel, S.-I. Nakaoka, Y. Niwa, T. Ono, D. Pierrot, B. Poulter, G. Rehder, L. Resplandy, E. Robertson, C. Rödenbeck, T. M. Rosan, J. Schwinger, C. Schwingshackl, R. Séférian, A. J. Sutton, C. Sweeney, T. Tanhua, P. P. Tans, H. Tian, B. Tilbrook, F. Tubiello, G. R. van der Werf, N. Vuichard, C. Wada, R. Wanninkhof, A. J. Watson, D. Willis, A. J. Wiltshire, W. Yuan, C. Yue, X. Yue, S. Zaehle, and J. Zeng, *Global carbon budget 2021*, Earth System Science Data, 14 (2022), pp. 1917–2005.

[8] M. J. Glotter, R. T. Pierrehumbert, J. W. Elliott, N. J. Matteson, and E. J. Moyer, *A Simple Carbon Cycle Representation for Economic and Policy Analyses*, Climatic Change, 126 (2014), pp. 319–335.

[9] C. A. Hartin, B. Bond-Lamberty, P. Patel, and A. Mundra, *Ocean acidification over the next three centuries using a simple global climate carbon-cycle model: projections and sensitivities*, Biogeosciences, 13 (2016), pp. 4329–4342.

[10] C. A. Hartin, P. Patel, A. Schwarber, R. P. Link, and B. P. Bond-Lamberty, *A simple object-oriented and open-source model for scientific and policy analyses of the global climate system – hector v1.0*, Geoscientific Model Development, 8 (2015), pp. 939–955.

[11] R. B. Jackson, M. Saunois, P. Bousquet, J. G. Canadell, B. Poulter, A. R. Stavert, P. Bergamaschi, Y. Niwa, A. Segers, and A. Tsuruta, *Increasing anthropogenic methane emissions arise equally from agricultural and fossil fuel sources*, Environmental Research Letters, 15 (2020), p. 071002.

[12] L. Kessler, *Estimating the economic impact of the Permafrost Carbon Feedback*, Climate Change Economics, 8 (2017), pp. 1–23.

[13] T. M. Lenton, J. Rockström, O. Gaffney, S. Rahmstorf, K. Richardson, W. Steffen, and H. J. Schellnhuber, *Climate tipping points-too risky to bet against*, (2019).

[14] A. H. MacDougall, C. A. Avis, and A. J. Weaver, *Significant contribution to climate warming from the permafrost carbon feedback*, Nature Geoscience, 5 (2012), p. 719–721.

[15] M. Meinshausen and S. Smith et al., *The rcp greenhouse gas concentrations and their extension from 1765 to 2500*, 2011.

[16] G. Myhre, E. J. Highwood, K. P. Shine, and F. Stordal, *New estimates of radiative forcing due to well mixed greenhouse gases*, Geophysical Research Letters, 25 (1998), pp. 2715–2718.

[17] G. Myhre, D. Shindell, F.-M. Bréon, W. Collins, J. Fuglestvedt, J. Huang, D. Koch, J.-F. Lamarque, D. Lee, B. Mendoza, T. Nakajima, A. Robock, G. Stephens, T. Takemura, and H. Zhang, *2013: Anthropogenic and Natural Radiative Forcing Supplementary Material*, in In Climate Change 2013: The Physical Science Basis. Contribution of Working Group I to the Fifth Assessment Report of the Intergovernmental Panel on Climate Change, T. F. Stocker, D. Qin, G.-K. Plattner, M. Tignor, S. K. Allen, J. Doschung, A. Nauels, Y. Xia, V. Bex, and P. M. Midgley, eds., Cambridge University Press, Cambridge, UK, 2013, pp. 659–740.

[18] R. T. Pierrehumbert, *Short-Lived Climate Pollution*, Annual Review of Earth and Planetary Sciences, 42 (2014), pp. 341–379.

[19] P. D. L. Ritchie, J. J. Clarke, P. M. Cox, and C. Huntingford, *Overshooting tipping point thresholds in a changing climate*, Nature, 592 (2021), pp. 517–523.

[20] J. Rogelj, P. Forster, E. Kriegler, C. Smith, and R. Séférian, *Estimating and tracking the remaining carbon budget for stringent climate targets*, Nature, 571 (2019), p. 335.

[21] T. Schneider von Deimling, M. Meinshausen, A. Levermann, V. Huber, K. Frieler, D. M. Lawrence, and V. Brovkin, *Estimating the near-surface permafrost-carbon feedback on global warming*, Biogeosciences, 9 (2012), pp. 649–665.

[22] W. Steffen, K. Richardson, J. Rockström, S. E. Cornell, I. Fetzer, E. M. Bennett, R. Biggs, S. R. Carpenter, W. de Vries, C. A. de Wit, C. Folke, D. Gerten, J. Heinke, G. M. Mace, L. M. Persson, V. Ramanathan, B. Reyers, and S. Sörlin, *Planetary boundaries: Guiding human development on a changing planet*, Science, 347 (2015).

[23] W. Steffen, J. Rockström, K. Richardson, T. M. Lenton, C. Folke, D. Liverman, C. P. Summerhayes, A. D. Barnosky, S. E. Cornell, M. Crucifix, J. F. Donges, I. Fetzer, S. J. Lade, M. Scheffer, R. Winkelmann, and H. J. Schellnhuber, *Trajectories of the Earth System in the Anthropocene*, Proceedings of the National Academy of Sciences, 115 (2018), pp. 8252–8259.

[24] Stocker, T.F., D. Qin, G.-K. Plattner, M. Tignor, S. Allena, J. Boschung, A. Nauels, Y. Xia, V. Bex, and P. M. (eds.), *Ipcc, 2013: Annex ii: Climate system scenario tables prather and m and g. flato and p. friedlingstein and c. jones and j.-f. lamarque and h. liao and p. rasch (eds.)*, tech. rep., In: Climate Change 2013: The Physical Science Basis. Contribution of Working Group I to the Fifth Assessment Report of the Intergovernmental Panel on Climate Change, Cambridge, United Kingdom and New York, NY, USA, 2014.

[25] S. Szopa, V. Vaik, B. Adhikary, and E. al, *Climate change 2021: The physical science basis.*

[26] T. Westerhold, N. Marwan, A. J. Drury, D. Liebrand, C. Agnini, E. Anagnostou, J. S. K. Barnet, S. M. Bohaty, D. D. Vleeschouwer, F. Florindo, T. Frederichs, D. A. Hodell, A. E. Holbourn, D. Kroon, V. Lauretano, K. Littler, L. J. Lourens, M. Lyle, H. Pälike, U. Röhl, J. Tian, R. H. Wilkens, P. A. Wilson, and J. C. Zachos, *An astronomically dated record of Earth's climate and its predictability over the last 66 million years*, Science, 369 (2020), pp. 1383–1387.

[27] D. L. Woodard, A. N. Shiklomanov, B. Kravitz, C. Hartin, and B. Bond-Lamberty, *A permafrost implementation in the simple carbon–climate model hector v.2.3pf*, Geoscientific Model Development, 14 (2021), pp. 4751–4767.